Inorganic Chemistry

Article

pubs.acs.org/IC

Understanding Ion Sensing in Zn(II) Porphyrins: Spectroscopic and Computational Studies of Nitrite/Nitrate Binding

Christi L. Whittington, William A. Maza, H. Lee Woodcock,* and Randy W. Larsen*

Department of Chemistry, University of South Florida, 4202 E. Fowler Avenue, Tampa, Florida 33620, United States

ABSTRACT: The development of effective sensor elements relies on the ability of a chromophore to bind an analyte selectively and then study the binding through changes in spectroscopic signals. In this report the ability of Zn(II) Tetraphenyl Porphyrin (ZnTPP) to selectively bind nitrite over nitrate ions is examined. The results of Benesi−Hildebrand analysis reveals that ZnTPP binds NO_2^- and NO_3^- ions with association constants of 739 ± 70 M^{-1} and 134 ± 15 M^{-1}, respectively. Interestingly, addition of a pyridine ligand to the fifth coordination site of the Zn(II) center enhances ion binding with the association constants increasing to 71,300 ± 8,000 M^{-1} and 18,900 ± 3,000 M^{-1} for nitrite and nitrate, respectively. Density functional theory calculations suggest a binding mechanism through which Zn(II)−porphyrin interactions are disrupted by ligand and base coordination to Zn(II), with Zn(II) having more favorable overlap with nitrite orbitals, which are less delocalized than nitrate orbitals. Overall, these provide new insights into the ability to tune the affinity and selectivity of porphyrin based sensors utilizing electronic factors associated with the central Zn(II) ion.

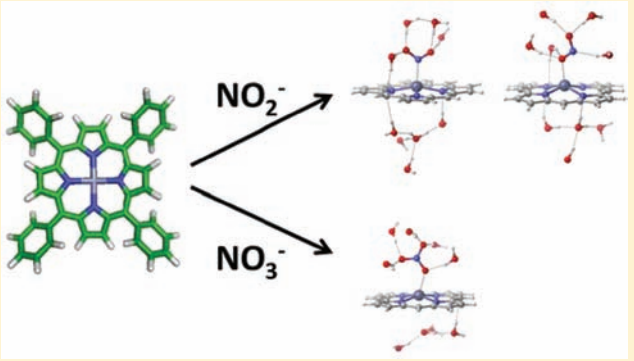

INTRODUCTION

The oxides of nitrogen including NO_2^- and NO_3^- are important ions in biology, the environment, and the food industry. In humans, NO_2^- has been identified as a biomarker for NO-synthase activity as well as a storage form of nitric oxide, being activated by deoxy hemoglobin.[1,2] In bacterial systems, NO_2^- is an important ion in the nitrogen cycle which converts NO_3^- to ammonium or vice versa.[3] The conversion of NH_4^+ to NO_3^- represents an intermediate step in nitrogen fixation and involves enzymes which catalyze assimilatory, respiratory, or dissimilatory reduction of NO_3^- to NO_2^-. Environmentally, NO_3^- based fertilizers (typically ammonium nitrate) have proven to be the most cost-effective method of nitrogen delivery to plants. However, the high water solubility of both NO_3^- and NO_2^- (produced as an intermediate in bacterial ammonification) have led to significant groundwater contamination.[4,5] This contamination has been identified as a serious health risk as NO_3^- consumption can lead to methemoglobinemia, a disorder in which methemoglobin builds up in the bloodstream.[6] Despite the obvious health risks, low concentrations of nitrates are commonly used in the food industry as preservatives.[7]

The ability to selectively sense nitrogen oxides has obvious environmental and health implications with a number of technologies having been developed for their detection. These include electrochemical detection, ion chromatography, HPLC, and various optical techniques.[8−11] One of the most common nitrite detection techniques is derivitization to append a chromophore that can then be identified colorimetrically or through fluorescence methods. In the case of nitrate, the anion is first reduced to nitrite followed by chemical modification and optical detection.[8] When a fluorescent sensor is used, concentrations as low as 10 nM can be determined. Electrochemical detection improves sensitivity over standard colorimetric analysis as well as increasing selectivity. HPLC methods coupled with optical techniques can improve detection limits to as low as 10 pM.[8]

In terms of optical detection, porphyrins represent attractive candidates for sensor elements. This is because the porphyrin macrocycle exhibits rich spectroscopic features including: (1) high molar extinction coefficients in both the near UV (up to ∼200 mM^{-1} cm^{-1}) and visible regions (up to ∼75 mM^{-1} cm^{-1}), (2) high fluorescence quantum yields (up to ∼0.2), and (3) the porphyrin core can accommodate a broad array of metals which in turn bind or catalytically degrade a wide variety of analytes, forming the basis for both optical and potentiometric sensor elements.[12−16] In addition, both free-base and metalloporphyrins can be functionalized at the periphery to enhance binding specificity.[17,18] Porphyrin based potentiometric sensing platforms have primarily utilized Mn(III) porphyrins for the detection of triiodie,[19] penicillin-G,[20] thiocyanate,[21] and diclofenac (a nonsteroidal anti-inflammatory drug used for the treatment of rheumatoid arthritis)[22] to name only a few.

Zn(II) porphyrins are of particular interest in sensor development as these chromophores exhibit significant fluorescence quantum yields, have long-lived triplet states,

Received: January 6, 2012
Published: April 5, 2012

dx.doi.org/10.1021/ic300039v | Inorg. Chem. 2012, 51, 4756−4762

Scheme 1. Possible Orientations of ZnP Complexes, 1−10

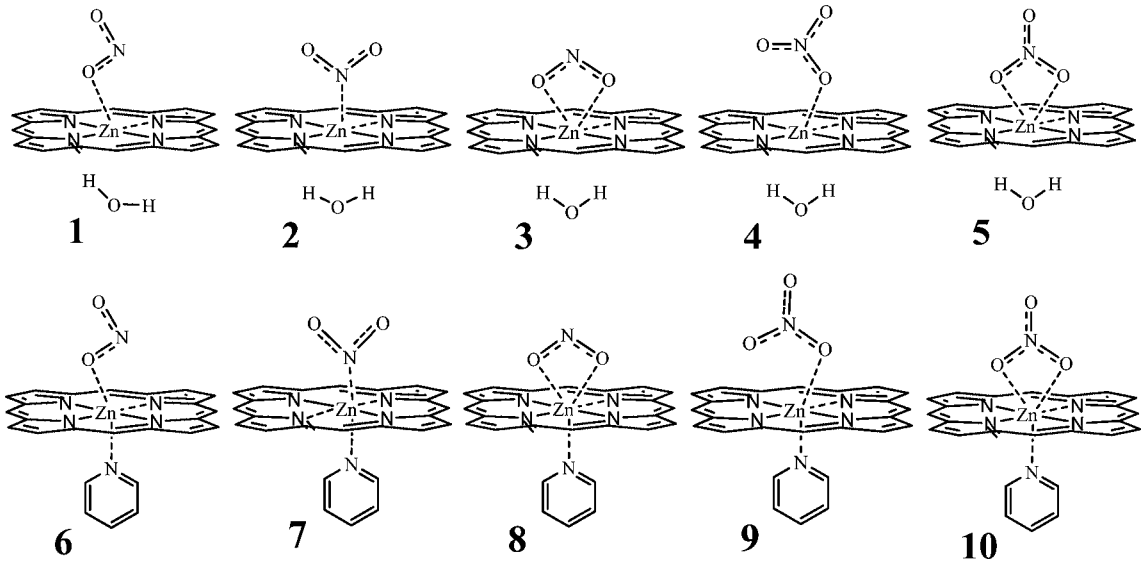

and can interact with a wide variety of axial ligands through the Zn(II) ion.[23−26] These chromophores have been shown to exhibit selectivity toward nitrogen- (amines) and oxygen-containing (tetrahydrofurans) compounds as well as other small molecules and ions.[27−29] The ability of Zn(II) porphyrins to bind small molecules allow these chromophores to be examined as sensor platforms for nitrite/nitrate detection. In the present study, experimental results demonstrating the preferential binding of NO_2^- over NO_3^- to the metalloporphyrin Zn(II) 5,10,15,20-tetraphenylporphyrin (ZnTPP) as well as the increase in binding affinity by 2 orders of magnitude in the presence of a proximal base, pyridine (Pyr), are presented. Further, computational evidence, from electronic structure calculations, is provided to elucidate the underlying effects that govern the observed binding affinities; for example, proximal base effects. Zn(II) porphine (ZnP) was used as a model for ZnTPP to examine the role of the central Zn(II) ion, the porphyrin macrocycle, and ligand orbital interactions on binding selectivity and affinity.

MATERIALS AND METHODS

All reagents and solvents including $NaNO_2$, $NaNO_3$, 2-propanol, methanol, and Zn(II) acetate ($Zn(OAc)_2$) were purchased and used as received from Sigma-Aldrich. Free-base 5,10,15,20-tetraphenyl porphyrin (H_2TPP) was synthesized according to literature methods.[30] ZnTPP was synthesized by dissolving H_2TPP in methanol with excess $Zn(OAc)_2$ and refluxing for 3−4 h. The progress of the reaction was monitored by UV−vis spectroscopy. Once the reaction was complete the methanol was evaporated off and the solid resuspended in ethyl acetate. The solution was washed three times with water to remove excess $Zn(OAc)_2$ and the organic layer collected and dried by rotary evaporation.

UV−vis absorption spectra were collected on a Shimadzu UV-2401PC spectrophotometer. Steady-state emission spectra were collected using an ISS PC1 single photon counting spectrofluorimeter. Samples were excited at 422 nm and emission data collected between 550 nm and 750 nm. Samples were prepared by diluting a small amount of ZnTPP stocks (prepared in 2-propanol) into a 7:3 2-propanol/water mixture (v/v) (sample porphyrin concentration <10 μM). Stock solutions of $NaNO_2$ (530 mM), $NaNO_3$ (520 mM), and pyridine (150 mM) stock solutions were prepared in water and titrated into samples of ZnTPP while mixing, using a magnetic stir-bar, and the spectra collected.

Restricted Kohn−Sham Density Functional Theory (DFT) calculations were performed with Q-Chem.[30] The coordinates for all calculations were obtained from the crystal structure of ZnTPP coordinated with pyridine (Pyr); the pyridine and functionality of the porphyrin ring was removed in Avogadro,[31] giving ZnP, which was then combinatorially complexed with ligands (NO_2^- and NO_3^-) and bases (Pyr and H_2O), resulting in complexes **1**−**10** (Scheme 1). DFT gas phase (GP) geometry optimization of each structure employed the M06-L exchange-correlation functional[32] with a 75,302 grid.[33] LANL2TZ basis functions with Effective Core Potentials (ECPs)[34] were applied to Zn(II), with the remaining atoms being described by the 6-31G* basis set.[35] This has been shown to be an effective combination for studying metal-porphyrin complexes.[36] To ensure that the optimization was not biased by initial ligand orientation, 180 degree rotations of both ligands parallel and perpendicular to the plane of the porphine ring were performed with optimizations carried out on each of these structures. In each case, the ligand adopted the orientations in Scheme 1.

Exclusion of complexes **3**, **5**, **8**, and **10** will be discussed in the Results and Discussion section. While analyzing minimized complexes **1**, **2**, **4**, **6**, **7**, and **9**, it became clear that GP modeling was insufficient for describing water coordination (**1**, **2**, **4**). Thus, quantum mechanical/molecular mechanical (QM/MM) geometry optimizations were performed using the Q-Chem/CHARMM interface.[30,37,38] Complexes **1**, **2**, and **4** were each solvated in a TIP3P water sphere (~700 H_2O molecules).[39,40] The ZnP chromophore, ligand (NO_2^-/NO_3^-), and base (Pyr/H_2O) constituted the QM region, treated at the B3LYP/6-31G* level of theory,[41,42] with the MM region consisting of the remaining water molecules. QM nonbonded parameters for ZnP and NO_2^-/NO_3^- were obtained from ZN, C, N, H, and O atom types from the standard CHARMM22 force field.[43]

Localized orbitals involved in binding were determined by Natural Bond Orbital (NBO)[44,45] analysis during the SP calculations. NBO assigns localized orbitals to molecules based upon bonds and lone pair electrons (lp), providing a bridge between molecular and atomic orbitals and facilitating analysis. Orbital stabilization energies (E_{orb}) related to stability gained from electron delocalization were extracted from NBO results. Specifically, interactions involved in ligand and base coordination to ZnP were used to analyze binding modes and affinities.

To probe solvation effects in **1**, **2**, and **4**, waters with a 3.2 Å donor−acceptor distance[46] to NO_2^- were selected and used to construct and evaluate a microsolvated complex. The GP quantum binding energy (ΔE_{HB}) was determined for each hydrogen bonded water for **1**, **2**, and **4** by calculating the total energy, moving each water out of interaction range (≥100 Å), and recalculating the total energy at

dx.doi.org/10.1021/ic300039v | Inorg. Chem. 2012, 51, 4756−4762

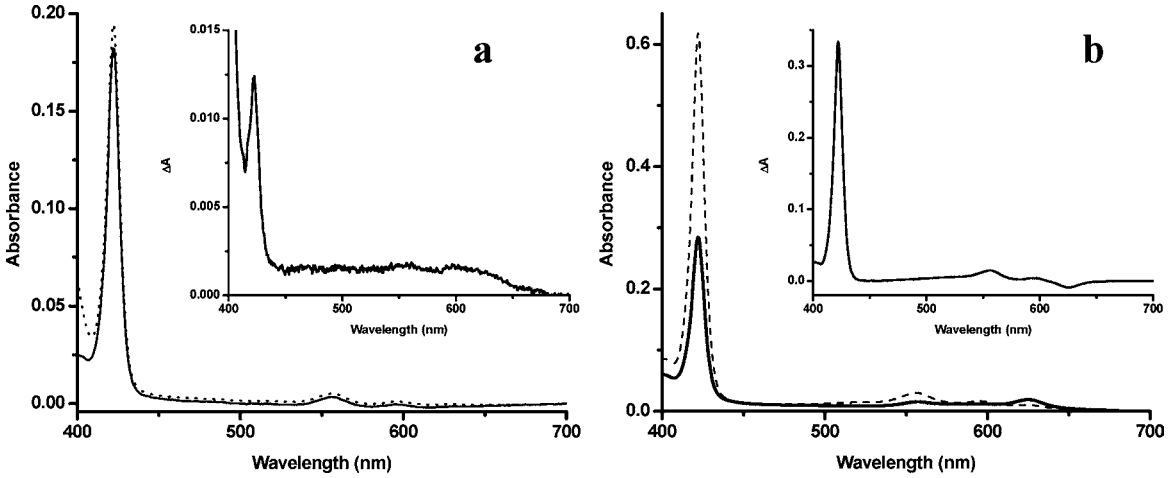

Figure 1. Absorption spectra of 10 μM ZnTPP in a 70% 2-propanol/water (v/v) solution containing: no NO_2^- or NO_3^- (solid line), (a) 31 mM NO_2^- (dotted line), and (b) 37 mM NO_3^- (dashed line). Insets show difference spectra of ZnTPP in the presence and absence of NO_2^- or NO_3^-.

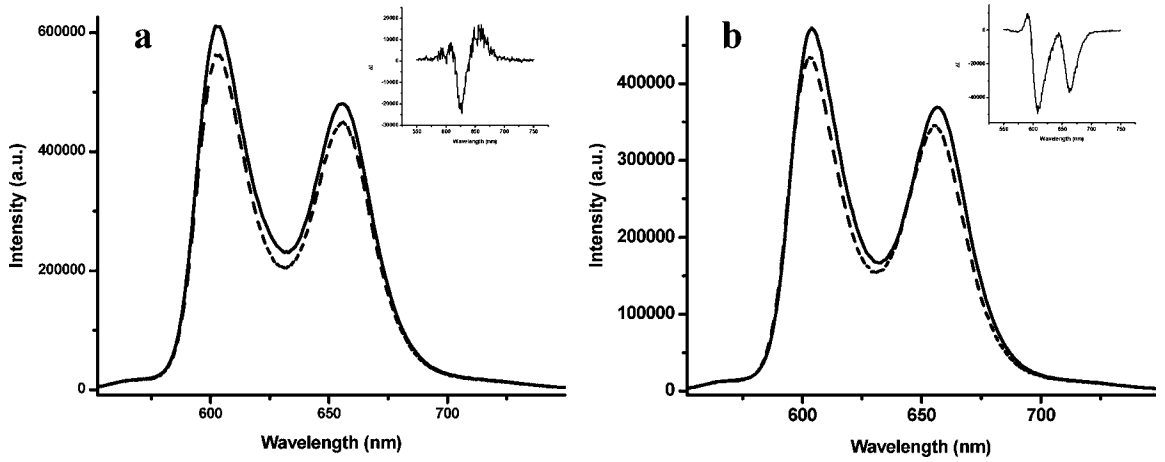

Figure 2. Steady-state emission spectra of a 10 μM ZnTPP in a 70% 2-propanol/water (v/v) solution containing: no NO_2^- or NO_3^- (solid line), (a) 31 mM NO_2^- (dotted line), and (b) 37 mM NO_3^- (dashed line). Insets show difference spectra of ZnTPP in the presence and absence of NO_2^- or NO_3^-.

the B3LYP/6-31G* level of theory with the Q-Chem/CHARMM interface.

RESULTS AND DISCUSSION

The absorption spectra of ZnTPP solubilized in the 7:3 (v/v) 2-propanol/water mixture displays transitions typical for Zn(II) porphyrins (Figure 1, dotted trace). Specifically, a symmetry allowed transition centered at 422 nm corresponding to the B-band, or Soret band, is observed as well as two transitions at 557 and 596 nm (Q-bands). Addition of NO_2^- or NO_3^- resulted in hyperchromic shifts in the absorption spectra (Figure 1 solid and dashed traces, respectively). Changes in the absorption spectra were plotted as a function of NO_2^- or NO_3^- ion concentration and fit using,[47]

$$\Delta A = \{K_a[X^-]/(1 + K_a[X^-])\}[\text{ZnTPP}]_0 \Delta\varepsilon_\lambda \quad (1a)$$

or, for emission data (Figure 2),

$$\Delta I = \{K_a[X^-]/(1 + K_a[X^-])\}(I_\infty - I_o) \quad (1b)$$

where $[\text{ZnTPP}]_0$ is the initial sample porphyrin concentration; $\Delta\varepsilon_\lambda$ is the change in molar extinction at probe wavelength λ (424 nm for both NO_2^- and NO_3^- binding to ZnTPP, 420 nm for NO_3^- binding to ZnTPP(Pyr), and 422 nm for NO_2^- binding to ZnTPP(Pyr)), I_o is the emission intensity in the absence of the anion, I_∞ is emission intensity at infinite concentration of the anion, and K_a is the association constant of a 1-to-1 interaction following the scheme:

$$\text{ZnTPP(L)} + X^- \overset{K_a}{\rightleftarrows} \text{ZnTPP(L)}(X^-) \quad (2)$$

where L is a proximal base (either H_2O or Pyr). In the absence of pyridine as a proximal base the K_a values from fits to eq 1a were found to be 739 ± 70 M^{-1} (ΔG° = −3.9 ± 0.1 kcal mol^{-1}) and 134 ± 15 M^{-1} (ΔG° = −2.9 ± 0.1 kcal mol^{-1}) for NO_2^- and NO_3^-, respectively (See Figure 3, Table 1). Steady-state emission data for both NO_2^- and NO_3^- binding to ZnTPP yields K_a values identical (within experimental error) to those obtained from the absorption data: 516 ± 193 M^{-1} and 116 ± 25 M^{-1} for NO_2^- and NO_3^-, respectively. Addition of pyridine to the ZnTPP solution, to give predominately the ZnTPP(Pyr) complex, resulted in an increase in binding affinity toward both NO_2^- and NO_3^- with K_a values of 71,300 ± 8,000 M^{-1} (ΔG° = −6.6 ± 0.1 kcal mol^{-1}) and 18,900 ± 3,000 M^{-1} (ΔG° = −5.9 ± 0.1 kcal mol^{-1}), respectively (Figure 4). Again, the association constants for both NO_2^- and NO_3^- binding to ZnTPP in the presence of pyridine obtained using emission data yields K_a values identical (within experimental error) to

dx.doi.org/10.1021/ic300039v | Inorg. Chem. 2012, 51, 4756−4762

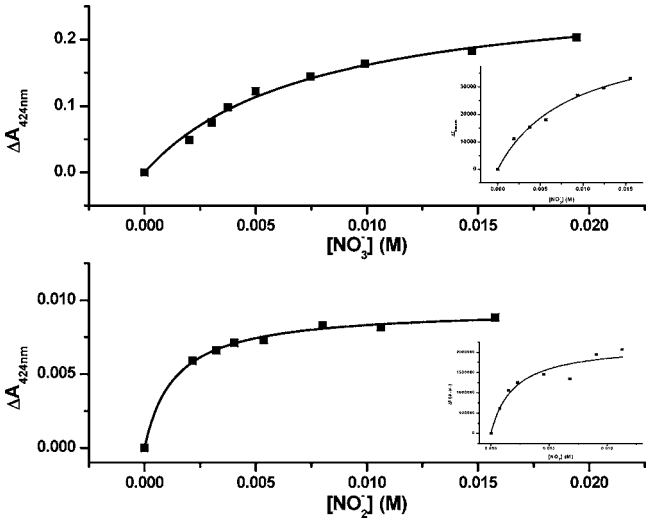

Figure 3. Change in steady-state absorption of ZnTPP at 424 nm as a function of (bottom) $[NO_2^-]$ and (top) $[NO_3^-]$. In each case the initial concentration of ZnTPP was 10 μM. Solid lines represent best fits to eq 1a. Insets for each show the change in steady-state emission of ZnTPP at 608 nm (λ_{exc} 422 nm); solid lines represent best fits to eq 1b.

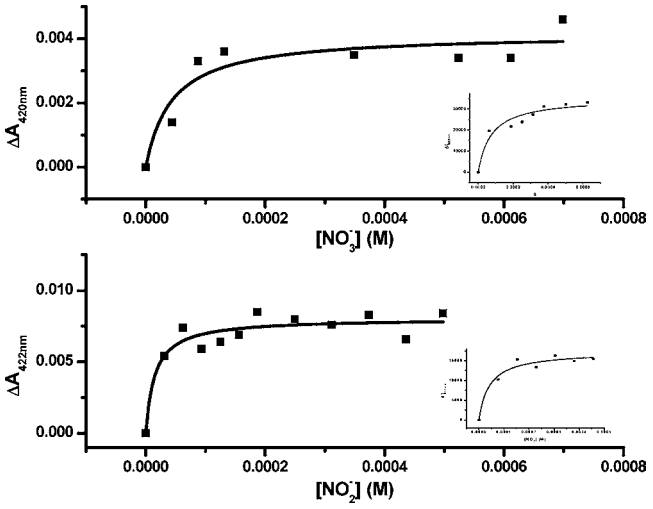

Figure 4. Change in steady-state absorption of 10 μM ZnTPP in the presence of 1 mM pyridine (to give predominantly the 5-coordinate ZnTPP(Pyr) complex) as a function of (bottom, changes monitored at 422 nm) $[NO_2^-]$ and (top, changes monitored at 420 nm) $[NO_3^-]$. Solid lines represent best fits to eq 1a. Insets for each show the change in steady-state emission of ZnTPP at 622 nm (λ_{exc} 422 nm); solid lines represent best fits to eq 1b.

those obtained from the absorption data: 79,200 ± 7,800 M^{-1} and 13,400 ± 5,200 M^{-1}, for NO_2^- and NO_3^-, respectively.

To characterize the selectivity of ZnTPP toward NO_2^-, orbital interactions that govern binding affinity have been examined computationally for the model ZnP complexes depicted in Scheme 1. There are three possible binding orientations for NO_2^-; single oxygen bound (**1**, **6**), nitrogen bound (**2**, **7**), and double oxygen bound (**3**, **8**); while NO_3^- has only two; single oxygen bound (**4**, **9**) and double oxygen bound (**5**, **10**). Figure 5 displays the geometry optimized complex **6**, in which the Zn(II) lies out of the porphine plane by 0.3−0.5 Å for both ligands (NO_2^-, NO_3^-) and either proximal base (Pyr, H_2O).[48]

Integral to understanding ion selectivity by Zn(II) porphyrins is knowing the correct binding modes of the ligands to the central Zn(II). The first modes examined were those with two oxygen atoms from the NO_2^-/NO_3^- bound to Zn(II) (**3**, **5**, **8**, **10**) in GP. Although this orientation allows for favorable interactions between the anions and the Zn(II), specifically electron donation from the π system on NO_2^-/NO_3^- to the unfilled Zn(4s) orbital, efficient solvent interactions seem unlikely. For example, the NO_2^- structures with two oxygen atoms bound to the Zn(II) (**3**, **8**) have only three likely hydrogen bond acceptor sites available to interact with solvent (water in this case) while conformations with a single oxygen atom bound to the Zn(II) (**1**, **2**, **6**, **7**) should have at least four available sites. Likewise for NO_3^-, there are

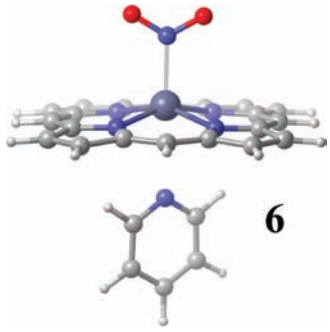

Figure 5. Geometry optimized structure of complex **6**. Zn(II) is out-of-plane toward NO_2^-.

more possible hydrogen bond acceptor sites for single oxygen bound orientations; five sites for **4** and **9** compared to four sites for **3** and **8**.

Although the orientations containing two oxygen atoms coordinated to the Zn(II) are energetically favorable, NO_2^- has two additional binding modes (**1**, **2**) that can be stabilized by solvent interactions. These modes along with NO_3^- (**4**) were examined through QM/MM minimization, with the QM region defined as ZnP, ligand (NO_2^-/NO_3^-) and the proximal base H_2O. In all three cases, the QM water molecule (i.e., base) reorients to participate in a solvent hydrogen bonding network. Additionally, the solvent interaction with the ligands differed

Table 1. Association Constants and Free Energies for NO_2^- and NO_3^- Binding to ZnTPP[a]

	ZnTPP		ZnTPP(Pyr)	
	K_a (M^{-1})	$\Delta G°$ (kcal/mol)	K_a (M^{-1})	$\Delta G°$ (kcal/mol)
NO_3^-	134 ± 15 (116 ± 25)	−2.9 ± 0.1	18,900 ± 3000 (13,400 ± 5,200)	−5.8 ± 0.1
NO_2^-	739 ± 70 (516 ± 193)	−3.9 ± 0.1	71,300 ± 8000 (79,200 ± 7,800)	−6.6 ± 0.1

[a]Data in parentheses were obtained from steady-state emission.

dx.doi.org/10.1021/ic300039v | Inorg. Chem. 2012, 51, 4756−4762

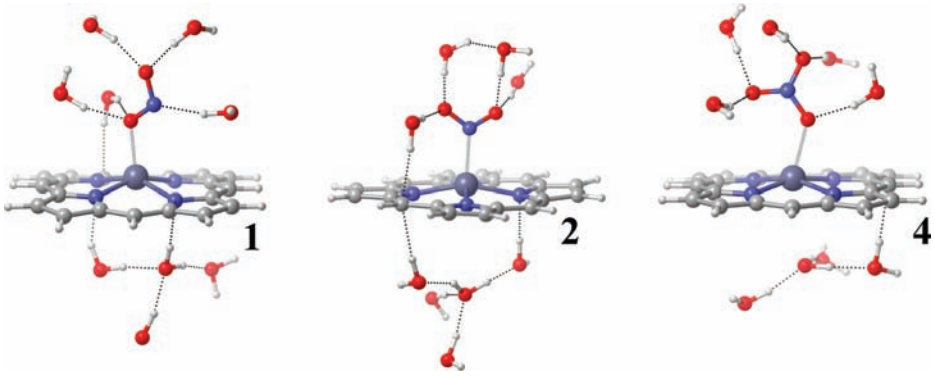

Figure 6. QM/MM optimized complexes **1**, **2**, and **4** with TIP3P waters hydrogen bonded to ligand, porphine, and base water.

between the three complexes examined. As predicted, **2** displayed four hydrogen bonds between NO_2^- and solvent with **4** having five. Surprisingly, **1** also exhibited five hydrogen bonds (only four were predicted) with the additional hydrogen bond to the Zn(II) coordinated oxygen (Figure 6).

To determine the extent of solvent stabilization in NO_2^-/NO_3^- binding the QM region and water molecules of interest were isolated and the hydrogen bond energy (E_{HB}) for each water was computed in GP (See methods, Table 2). The hydrogen bonded waters contribute a total of 45.7, 35.6, and 43.5 kcal/mol of E_{HB} stabilization for **1**, **2**, and **4**, respectively. As Zn(II) is a closed shell metal, the primary Zn(II) interactions observed are with the Zn(4s) orbital; however, some Zn(3d) orbital interactions are seen. Analysis of the microsolvated structures reveal an E_{orb} of 29.2 and 35.1 kcal/mol due to ligand (L) to Zn(II) electron donation (L→Zn(II)) for **1** and **2**, respectively. This indicates that the nitrogen bound structure (**2**) would be preferred in the absence of microsolvation. However, inclusion of microsolvation interactions elucidates the stabilizing role solvent plays on the complexes. For example, **1** has five hydrogen bonds involving solvent waters relative to four in **2**. This results in ∼10 kcal/mol of additional E_{HB} stabilization and shifts the predicted favorability from **2** to **1** despite the ∼6 kcal/mol greater stabilization due to L→Zn(II) interactions in **2** (Table 2). To further explain the microsolvation interactions, the L→H_2O and H_2O→H_2O orbital stabilizations were examined via NBO analysis for complexes **1**, **2**, and **4**. Again, the results demonstrate competing effects; the L→H_2O stabilization, which is ∼5 kcal/mol more favorable for **2**, is offset by more favorable H_2O→H_2O interactions (∼7 kcal/mol) for **1**. These results indicate that the oxygen bound structure (**1**) is preferred largely because of enhanced solvation effects, not more favorable L→Zn(II) interactions.

To understand the selectivity of ZnP for NO_2^- relative to NO_3^-, NBO analysis was again utilized. The E_{orb} results for **1**, **4**, **6**, and **9** are reported in Table 3 and are consistent with the experimental observation of NO_2^- binding selectively over NO_3^-. First, the NBO results suggest that H_2O→Zn(II) interactions do not contribute significantly to stabilization with H_2O as the proximal base (**1**, **4**). Thus, the orbital interactions between both the porphine (P) ring and the NO_2^-/NO_3^- ligands with the Zn(II) ion are responsible for the observed selectivity. In contrast, with pyridine as the proximal base (**6**, **9**) additional interactions between Zn(II) and both the pyridine nitrogen lp and the aromatic ring π electrons are observed. These interactions result in increased stabilization for both NO_2^- and NO_3^- by ∼3 kcal/mol due to pyridine lp and ∼1−1.5 kcal/mol from π electron donation into the Zn(4s). These stabilizations combined with L→Zn(II) interactions described above account for ∼10 kcal/mol of increased stability for **6** relative to **1** and ∼19 kcal/mol of increased stability for **9** relative to **4**. The stability enhancement by pyridine as a proximal base ($\Delta E_{Pyr} = \Delta E_{9-4} - \Delta E_{6-1}$ = ∼9 kcal/mol) can be largely rationalized by examining L→Zn(II) stabilization energies: $\Delta(L\rightarrow Zn)_{6-1}$ = 5.4 kcal/mol and $\Delta(L\rightarrow Zn)_{9-4}$ = 14.7 kcal/mol. The underlying cause of this shift is multifaceted beginning with the P→Zn(II) interactions, where $\Delta(P\rightarrow Zn)_{6-1}$ = −17.4 kcal/mol and $\Delta(P\rightarrow Zn)_{9-4}$ = −29.7 kcal/mol. The

Table 2. Binding Energies (E_{HB}) of Hydrogen Bonded Water Molecules in Gas Phase and Stabilization Energies (E_{orb}) from NBO Analysis of Single Point Energy Calculations, Depicted in Figure 6[a]

structure	1	2	4
number of H_2O (n)	5	4	5
		E_{HB} (kcal/mol)	
nH_2O	45.7	35.6	43.5
average	9.1	8.9	8.7
		E_{orb} (kcal/mol)	
nH_2O(lp)-nH_2O(σ^*)	15.6	8.3	1.5
L(lp) → Zn(4s)	29.2	35.1	19.6
Zn(3d) → L(σ^*)	0.2	0.8	0.3
L(lp) → nH_2O(σ^*)	79.7	85.0	77.2
total H_2O	95.3	93.3	78.7

[a]Structures included no base (Pyr or H_2O). L is NO_2^- or NO_3^-. Positive E_{HB} and E_{orb} values are favorable.

Table 3. Stabilization Energies (E_{orb}) from NBO Analysis of Single Point Energy Calculations in Gas Phase[a]

	E_{orb} (kcal/mol)			
orbital interaction	1	4	6	9
L(lp) → Zn(4s)	38.5	27.0	43.9	41.7
Zn(4s) → L(σ^*)	5.8	0.3	3.6	0.1
B(lp,π) → Zn(4s)	N/A	N/A	4.4	4.0
Zn(4s) → B(σ^*)	N/A	N/A	1.6	0.0
P(lp) → Zn(4s)	160.0	173.3	142.6	143.6
Zn(4s) → P(σ^*)	38.4	2.9	17.4	2.1
P(π,lp) → B(σ^*)	6.6	0.0	1.6	2.0

[a]L is NO_2^- or NO_3^-, B is H_2O or Pyr, and P is porphine. Positive E_{orb} values are favorable.

dx.doi.org/10.1021/ic300039v | Inorg. Chem. 2012, 51, 4756−4762

P→Zn(II) interaction is disrupted by the binding of pyridine thus allowing the Zn(II) ion to accept additional electron density, increasing L→Zn(II) stabilization and therefore binding affinity.

To further examine this disruption, Zn(II) back-bonding to the ligand, base, and porphine was examined. Upon reduction of Zn(II)→P back-bonding, L−Zn(II) (L→Zn(II) and Zn-(II)→L) stabilization was reduced as well as binding affinity. For example, when comparing **1** and **4** the Zn(II)→P back-bonding was decreased by ∼36 kcal/mol and the L−Zn(II) interaction was reduced by ∼17 kcal/mol. Likewise for **6** and **9**, an ∼15 kcal/mol decrease in back-bonding was accompanied by an ∼6 kcal/mol drop in L−Zn(II) stabilization. Zn(II)→L (**1**, **6**) and Zn(II)→B (**6**) back-bonding are more favorable for NO_2^- complexes. These trends mirror the experimental binding affinities and yield insight into selectivity. The NO_2^- orbitals are less delocalized than NO_3^-, giving more favorable orbital overlap between Zn(4s) and NO_2^- as well as disrupting P−Zn(II) interactions.

Since base (B) interactions with Zn(II) play such a significant role in both binding and selectivity, the role of water as the "base" and the orbital effects of the bases on the electronic properties of the Zn(II) ion have been examined. The QM/MM structures revealed two possible roles for water; one in which the water molecule is completely noninteracting and a second in which the water molecule interacts with porphine nitrogen and carbon atoms (Figure 6). In the former the base water was fully saturated by the hydrogen bonding network of the solvent environment and had no orbital interactions with the Zn(II), porphine, or ligand. The latter case saw nitrogen or carbon interactions where π and lp electron density was donated into σ^* orbitals on the water molecule. The P→B interaction in complex **1** was determined to be 6.6 kcal/mol, enthalpically competitive with standard water−water hydrogen bonds.

CONCLUSION

It has been demonstrated that ZnTPP selectively binds nitrite over nitrate because of more favorable ligand−Zn(II) orbital overlap, both π-type interactions from the ligand to the Zn(II) ion and subsequent back-bonding to the ligand. For either ligand, the preferred binding mode is such that a single oxygen is bound to the Zn(II) (**1**, **6**). With water in the proximal base position an orientation is established in which the water molecule engages in a hydrogen bonding network with neighboring solvent water molecules as well as interactions involving porphine π orbitals. With either pyridine or water as a proximal base, electron donation from the porphine ring to the Zn(II) ion is less stabilizing for nitrite than nitrate, and subsequently more back-bonding between Zn(II) and the porphine ring takes place with nitrite coordinated to the Zn(II). Greater ligand and/or base π electron donation onto the Zn(4s) destabilizes the porphine−Zn(II) interaction. Interestingly, the ligand→Zn(II) π interaction is more favorable with pyridine than water, explaining why, in solution, there is higher ligand binding affinity with pyridine addition. Therefore, binding affinities should be maximized when favorable ligand−Zn(II) and disrupting porphine−Zn(II) interactions exist. This information may facilitate the novel design of porphyrin frameworks to bind and detect small molecules.

AUTHOR INFORMATION

Corresponding Author

*E-mail: hlw@mail.usf.edu (H.L.W.), rwlarsen@usf.edu (R.W.L.).

Notes

The authors declare no competing financial interest.

ACKNOWLEDGMENTS

The authors would like to acknowledge the use of the services provided by Research Computing, University of South Florida, the Department of Defense−Defense Threat Reduction Agency (DoD-DTRA) through HDTRA1-08-C-0035, NIH/NHLBI (1K22HL088341-01A1), and the University of South Florida (start-up) for funding.

REFERENCES

(1) Ignarro, L. J.; Fukuto, J. M.; Griscavage, J. M.; Rogers, N. E.; Byrns, R. E. *Proc. Natl. Acad. Sci. U.S.A.* **1993**, *90*, 8103−8107.
(2) Batina., P.; Fritsch, P.; de Saint Blanquat, G.; Mitjavila, M. T. *Food Addit. Contam.* **1990**, *7* (Suppl1), S145−S149.
(3) Moreno-Vivián, C.; Cabello, P.; Martínez-Luque, M.; Blasco, R.; Castillo, F. *J. Bacteriol.* **1999**, *181*, 6573−6584.
(4) Bukowski, J.; Somers, G.; Bryanton, J. *J. Occup. Environ. Med.* **2001**, *43*, 377−383.
(5) Cedergren, M. I.; Selbing, A. J.; Lofman, O.; Källen, B. *Environ. Res.* **2002**, *89*, 124−130.
(6) Fewtrell, L. *Environ. Health Perspect.* **2004**, *112*, 1371−1374.
(7) Rahman, S. *Handbook of Food Preservation*, 2nd ed.; CRC Press: Boca Raton, FL, 1999.
(8) Moorcroft, M. J.; Davis, J.; Compton, R. G. *Talanta.* **2001**, *54*, 785−803.
(9) Salimi, A.; Noorbakhash, A.; Karonian, F. S. *Int. J. Electrochem. Sci.* **2006**, *1*, 435−446.
(10) Ito, K.; Takayama, Y.; Makabe, N.; Mitsui, R.; Hirokawa, T. *J. Chromatogr., A.* **2005**, *1083*, 63−67.
(11) Ensafi, A. A.; Chamjangali, M. A. *Spectrochim. Acta, Part A* **2003**, *59*, 2897−2903.
(12) Gorski, L.; Malinowska, E.; Parzuchowski, P.; Zhang, W.; Meyerhoff, M. E. *Electroanalysis* **2003**, *15*, 1229−1235.
(13) Malinowska, E.; Niedziolka, J.; Meyerhoff, M. E. *Anal. Chim. Acta* **2001**, *432*, 67−78.
(14) Gao, D.; Gu, J.; Yu, R.-Q.; Zheng, G.-D. *Analyst.* **1995**, *120*, 499−502.
(15) Di Natale, C.; Macagnano, A.; Repole, G.; Saggio, G.; D'Amico, A.; Paolesse, R.; Boschi, T. *Mater. Sci. Eng., C* **1998**, *5*, 209−215.
(16) Beer, P. D.; Cormode, D. P.; Davis, J. J. *Chem. Commun.* **2004**, *4*, 414−415.
(17) Chen, Y.; Fields, K. B.; Zhang, X. P. *J. Am. Chem. Soc.* **2004**, *126*, 14718−14719.
(18) Rose, E.; Quelquejeu, M.; Pandian, R. P.; Lecas-Nawrocka, A.; Vilar, A.; Ricart, G.; Collman, J. P.; Wang, Z.; Straumanis, A. *Polyhedron* **2000**, *19*, 581−586.
(19) Suzuki, H.; Nakagawa, H.; Mifune, M.; Saito, Y. *Anal. Sci.* **1993**, *9*, 351−354.
(20) Santos, E. M. G.; Araújo, A. N.; Couto, C. M. C. M.; Montenegro, M. C. B. S. M.; Kejzlarová, A.; Solich, P. *J. Pharm. Biomed. Anal.* **2004**, *36*, 701−709.
(21) Vlascici, D.; Bizerea Spiridon, O.; Făgădar-Cosma, E. *J. Optoelectron. Adv. Mater.* **2006**, *8*, 883−887.
(22) Arancibia, J. A.; Boldrini, M. A.; Escandar, G. M. *Talanta.* **2000**, *52*, 261−268.
(23) Cole, S. J.; Curthoys, G. C.; Magnusso, E. A.; Phillips, J. N. *Inorg. Chem.* **1972**, *11*, 1024−1028.
(24) Zhang, Y.; Yang, R. H.; Liu, F.; Li, K. A. *Anal. Chem.* **2004**, *76*, 7336.
(25) Barkigia, K. M.; Berber, M. D.; Fajer, J.; Medforth, C. J.; Renner, M. W.; Smith, K. M. *J. Am. Chem. Soc.* **1990**, *112*, 8851−8857.

(26) Whitten, D. G. *Res. Chem. Intermed.* **1978**, *2*, 107−138.
(27) Schauer, C. K.; Anderson, O. P.; Eaton, S. S.; Eaton, G. R. *Inorg. Chem.* **1985**, *24*, 4082−4086.
(28) Prasad, R.; Gupta, V. K.; Kumar, A. *Anal. Chim. Acta* **2004**, *508*, 61−70.
(29) Sanders, J. K. M.; Bampos, N.; Clyde-Watson, Z.; Darling, S. L.; Hawley, J. C.; Kim, H. J.; Mak, C. C.; Webb, S. J. *The Porphyrin Handbook*; Academic Press: San Diego, CA, 2000; Vol. 3.
(30) Shao, Y.; Fusti−Molnar, L.; Jung, Y.; Kussmann, J.; Ochsenfeld, C.; Brown, S. T.; Gilbert, A. T. B.; Slipchenko, L. V.; Levchenko, S. V.; O'Neill, D. P.; DiStasio, R. A., Jr.; Lochan, R. C.; Wang, T.; Beran, G. J. O.; Besley, N. A.; Herbert, J. M.; Lin, C. Y.; Voorhis, T. V.; Chien, S. H.; Sodt, A.; Steele, R. P.; Rassolov, V. A.; Maslen, P. E.; Korambath, P. P.; Adamson, R. D.; Austin, B.; Baker, J.; Byrd, E. F. C.; Daschel, H.; Doerksen, R. J.; Dreuw, A.; Dunietz, B. D.; Dutoi, A. D.; Furlani, T. R.; Gwaltney, S. R.; Heyden, A.; Hirata, S.; Hsu, C.-P.; Kedziora, G.; Khaliullin, R. Z.; Klunzinger, P.; Lee, A. M.; Lee, M. S.; Liang, W.; Lotan, I.; Nair, N.; Peters, B.; Proynov, E. I.; Pieniazek, P. A.; Rhee, Y. M.; Ritchie, J.; Rosta, E.; Sherrill, C. D.; Simmonett, A. C.; Subotnik, J. E.; Woodcock, H. L., III; Zhang, W.; Bell, A. T.; Chakraborty, A. K.; Chipman, D. M.; Keil, F. J.; Warshel, A.; Hehre, W. J.; Schaefer, H. F., III; Kong, J.; Krylov, A. I.; Gill, P. M. W.; Head-Gordon, M. *Phys. Chem. Chem. Phys.* **2006**, *8*, 3172−3191.
(31) Avogadro: an open-source molecular builder and visualization tool. Version 1.0.3. (http://avogadro.openmolecules.net/).
(32) Zhao, Y.; Truhlar, D. G *J. Chem. Phys.* **2006**, *125* (194101), 1−18.
(33) Wheeler, S. E.; Houk, K. N. *J. Chem. Theory Comput.* **2010**, *6*, 395−404.
(34) Roy, L. E.; Hay, J.; Martin, R. L. *J. Chem. Theory Comput.* **2008**, *4*, 1029−1031.
(35) Francl, M. M.; Pietro, W. J.; Hehre, W. J.; Binkley, J. S.; Gordon, M. S.; DeFrees, D. J.; Pople, J. A. *J. Chem. Phys.* **1982**, *77*, 3654−2665.
(36) Belof, J. L.; Cioce, C. R.; Xu, X.; Zhang, X. P.; Space, B.; Woodcock, H. L. *Organometallics* **2011**, *30*, 3739−2746.
(37) Brooks, B. R.; Brooks, C. L., III; Mackerell, A. D.; Nilsson, L.; Petrella, R. J.; Roux, B.; Won, Y.; Archontis, G.; Bartels, C.; Boresch, S.; Caflisch, A.; Caves, L.; Cui, Q.; Dinner, A. R.; Feig, M.; Fischer, S.; Gao, J.; Hodoscek, M.; Im, W.; Kuczera, K.; Lazaridis, T.; Ma, J.; Ovchinnikov, V.; Paci, E.; Pastor, R. W.; Post, C. B.; Pu, J. Z.; Schaefer, M.; B. Tidor, B.; Venable, R. M.; Woodcock, H. L., III; Wu, X.; Yang, W.; York, D. M.; Karplus, M. *J. Comput. Chem.* **2009**, *30*, 1545−1615.
(38) Woodcock, H. L., III; Hodoscek, M.; Gilbert, A. T. B.; Gill, P. M. W.; Schaefer, H. F.; Brooks, B. R. *J. Comput. Chem.* **2007**, *28*, 1485−1502.
(39) Miller, B. T.; Singh, R. P.; Klauda, J. B.; Hodoscek, M.; Brooks, B. R.; Woodcock, H. L. *J. Chem. Inf. Model.* **2008**, *48*, 1920−1929.
(40) Jorgensen, W. L.; Chandrasekhar, J.; Madura, J. D.; Impey, R. W.; Klein, M. L. *J. Chem. Phys.* **1983**, *79*, 926−935.
(41) Becke, A. D. *J. Chem. Phys.* **1993**, *98*, 5648−5652.
(42) Lee, C.; Yang, W.; Parr, R. G. *Phys. Rev. B.* **1988**, *37*, 785−789.
(43) MacKerell, A. D., Jr.; Bashford, D.; Bellott, M.; Dunbrack, R. L., Jr.; Evanseck, J. D.; Field, M. J.; Fischer, S.; Gao, J.; Guo, H.; Ha, S.; Joseph-McCarthy, D.; Kuchnir, L.; Kuczera, K.; Lau, F. T. K.; Mattos, C.; Michnick, S.; Ngo, T.; Nguyen, D. T.; Prodhom, B.; Reihe, W. E., III; Roux, B.; Schlenkrich, M.; Smith, J. C.; Stote, R.; Straub, J.; Watanabe, M.; Wiórkiewicz-Kuczera, J.; Yin, D.; Karplus, M. *J. Phys. Chem. B* **1998**, *102*, 3586−3616.
(44) Glendening, E. D.; Badenhoop, J. K.; Reed, A. E.; Carpenter, J. E.; Bohmann, J. A.; Morales, C. M.; Weinhold, F. *NBO 5.0*; Theoretical Chemistry Institute, University of Wisconsin: Madison, WI, 2001.
(45) Foster, J. P.; Weinhold, F. *J. Am. Chem. Soc.* **1980**, *102*, 7211−7218.
(46) Humphrey, W.; Dalke, A.; Schulten, K. *J. Molec. Graphics.* **1996**, *14*, 33−38.
(47) Benesi, H. A.; Hildebrand, J. H. *J. Am. Chem. Soc.* **1949**, *71*, 2703−2707.
(48) Legault, C. Y. *CYLview*, 1.0b; Université de Sherbrooke: Québec, Canada, 2009 (http://www.cylview.org).